In situ and lidar observations of subvisible cirrus clouds during TC4

Sean Davis[1,2], Dennis Hlavka[3], Eric Jensen[4], Karen Rosenlof[1], Sebastian Schmidt[5], Stephan Borrmann[6,7], Wiebke Frey[6], Paul Lawson[8], Holger Voemel[9], T.P. Bui[4]

[1] NOAA Earth System Research Laboratory (ESRL), Chemical Sciences Division, Boulder, CO

[2] Cooperative Institute for Research in Environmental Sciences (CIRES), University of Colorado at Boulder, Boulder, CO

[3] Science Systems and Applications, Inc. (SSAI), Greenbelt, MD

[4] NASA Ames Research Center, Moffett Field, CA

[5] Laboratory for Atmospheric and Space Physics (LASP), University of Colorado at Boulder, Boulder, CO

[6] Institute for Physics of the Atmosphere, Johannes-Gutenberg University, Mainz, Germany

[7] Particle Chemistry Department, Max-Planck Institute for Chemistry, Mainz Germany

[8] Stratton Park Engineering Company (SPEC), Inc., Boulder, CO

[9] Deutscher Wetterdienst, Meteorologisches Observatorium Lindenberg, Lindenberg, Germany

Abstract

During the Tropical Composition, Clouds, and Climate Coupling (TC4) experiment in July-August 2007, the NASA WB-57 and ER-2 aircraft made unprecedented coordinated flights through an extremely tenuous subvisible cirrus (SVC) layer off the Pacific Coast of Central America. The ER-2 aircraft was equipped with a remote sensing payload that included the cloud physics lidar (CPL). The WB-57 payload included cloud microphysical and trace gas measurements, and the aircraft made four vertical profiles through the SVC layer shortly after the ER-2 flew over. The in situ and remotely sensed data are used to quantify the meteorological and microphysical properties of the SVC layer, and these data are compared to the limited set of in situ SVC measurements that have been made to date in previous field campaigns. It is found that the layer encountered was particularly tenuous, with optical depths (τ) between about 10^{-4} and 10^{-3}. From the in situ and other meteorological data, radiative heating rate perturbations of ~ 0.01 – 0.1 K day^{-1} are calculated. These heating rates are smaller than several previous estimates, consistent with the smaller τ in the present study. A climatology of SVC properties from the CPL data indicates that this cloud was optically thinner than most other SVC measurements during TC4. SVC with properties similar to the one presented here are below the detection limit of space-based lidars such as CALIPSO, and the TC4 climatology suggests that a large fraction of SVC will be unaccounted for in global studies using that data.

1. Introduction

Cirrus clouds play an important role in Earth's radiative energy balance, and may contribute either a positive or negative radiative effect depending on their microphysical properties [e.g., *Fu and Liou*, 1993; *Stephens et al.*, 1990]. Within the broader category of cirrus clouds, sibvisible cirrus clouds (SVC, $\tau < 0.03$) have been found to have a net positive radiative effect on the top-of-atmosphere energy budget due to their infrared "greenhouse" effect outweighing their solar "albedo" effect [*Comstock et al.*, 2002; *Fu and Liou*, 1993; *McFarquhar et al.*, 2000]. Similarly, thin cirrus ($\tau < 0.3$), which include SVC, have been estimated to make a significant contribution to the global TOA radiation budget through their reduction of OLR [*Haladay and Stephens*, 2009].

In addition to their radiative importance, tropical SVC may also be involved in dehydration and radiatively-driven lofting of air as it ascends through the tropical uppermost troposphere into the stratosphere [*Corti et al.*, 2006; *Jensen et al.*, 1996; *Luo et al.*, 2003], thereby affecting the rates of transport of chemical constituents from convective detrainment levels up to the stratosphere. It has also been shown that SVC near the tropical tropopause can effectively regulate the humidity of air entering the stratosphere, which in turn affects the radiative budget and stratospheric ozone chemistry [*Dvortsov and Solomon*, 2001; *Forster and Shine*, 2002].

Compared to other cloud types, very few in situ measurements have been made of tropical subvisible cirrus because of their high altitudes (> 15 km), which necessitate the use of specialized high-altitude research aircraft. As such, the microphysical and radiative properties of these clouds are not well constrained. The only known in situ tropical SVC measurements at the time of writing are from the tropical Western Pacific in December 1973 [*Heymsfield*, 1986; *McFarquhar et al.*, 2000], the Indian Ocean during APE-THEOSO in February and March 1999 [*Luo et al.*, 2003; *Thomas et al.*, 2002], tropical West Africa during the AMMA campaign, and the tropical Eastern Pacific during CR-AVE in 2006 [*Lawson et al.*, 2008]. The SVC measurements presented below were taken in the same region as those from CR-AVE, except that these measurements were taken in August when the tropopause is relatively warm, as opposed to January and February for CR-AVE when the tropopause was very cold.

Overall, the previous in situ measurements of SVC indicate relatively consistent microphysical properties, with thicknesses < 1 km, ice concentrations ~ 10 – 100 L^{-1}, particle effective radii ~ 10 - 20 μm, extinctions ~ $10^{-4} – 10^{-3}$ km^{-1}, and IWC $10^{-4} – 10^{-3}$ g m^{-3} (~ 0.1 – 1 ppmv). However, it was found in *Lawson et al.* [2008] that the CR-AVE SVC were comprised of significantly different ice crystal habits than the W. Pacific SVC. The CR-AVE ice crystals were primarily quasi-spherical, whereas the W. Pacific SVC contained mostly columnar and trigonal plates. Furthermore, the CR-AVE SVC were also found to contain crystals larger than 50 μm, which did not exist in the W. Pacific data set (habit and particle size measurements capable of measuring crystals larger than 23 μm were unavailable during APE-THEOSO). The CR-AVE measurements bring up the possibility that geographic, seasonal, and/or long-term (i.e., climate change-related) differences in the microphysical properties of SVC exist, and also call into question some of the formation mechanisms needed for these clouds [*Jensen et al.*, 2008].

In this paper, we present a case study involving coordinated in situ and remote-sensing SVC measurements from the NASA ER-2 and WB-57 aircraft taken during the Tropical Composition, Clouds, and Climate Coupling (TC4) experiment in August 2007. The subvisible cirrus data presented in this paper represent a unique set of measurements that allow us to assess the microphysical and radiative properties of this cloud. In the next section, we present the in situ and remote sensing data from this SVC cloud encounter. The in situ microphysical data are compared to previous in situ measurements in tropical near-tropopause SVC. Then, the radiative heating rates and particle mass fluxes are calculated for this cloud and the implications for the dehydration potential of these clouds is discussed. Finally, aircraft-based lidar data are used to provide regional statistics of SVC in the equatorial Eastern Pacific during the TC4 campaign.

2. Data

The Tropical Composition, Clouds and Climate Coupling (TC4) campaign was based out of San Jose, Costa Rica during July and August 2007 [*Toon et al.*, this issue]. Three NASA research aircraft took part in this mission: the NASA DC-8 (low- to mid-troposphere), WB-57 (TTL region), and ER-2 (lower stratosphere). The DC-8 and WB-57 were equipped with in situ and remote sensing measurements, whereas the ER-2 contained a remote sensing payload that included the "A-train" simulator instruments such as the MODIS airborne simulator (MAS) and the Cloud Physics Lidar (CPL) [*McGill et al.*, 2002].

Throughout TC4, various combinations of these aircraft flew along coordinated tracks for the purposes of providing a complete set of measurements of the chemical, microphysical, and radiative environment. This paper focuses on one such flight from 6 August in which the three aircraft flew along a NE-SW flight leg from San Jose, Costa Rica towards the Galapagos islands (see Figure 1).

On this day, the ER-2 flew outbound from San Jose, Costa Rica, and a subvisible cirrus cloud was observed at ~16.5 km from ~12:45 – 13:15 UT in the preliminary CPL data that was transmitted to the mission operations facility in real time. This allowed the mission scientists to direct the WB-57 to the SVC layer approximately 45 minutes afterwards, where it performed several up-and-down "porpoise" maneuvers, ultimately making four passes through the SVC layer.

Measurements used in this study that were made from the WB-57 include water vapor, cloud microphysical, and meteorological data. Water vapor data used here are from the JPL Laser Hygrometer [JLH, *May*, 1998] and Harvard Lyman-α photofragment fluorescence hygrometer [HW, *Weinstock et al.*, 1994]. Cloud microphysical data are from the Cloud Particle Imager [CPI, *Lawson et al.*, 2001] and 2D-S [*Lawson et al.*, 2006]. The CPI images particles larger than 10 μm with 2.3 μm pixel resolution, and the 2D-S images particles from 10 μm - 8 mm with 10 μm resolution. Finally, pressure and temperature measurements with an accuracy of ± 0.25 hPa and ± 0.25 K, respectively, are provided by the meteorological measurement system [MMS, *Scott et al.*, 1990].

An overview time series plot of the ER-2 CPL and WB-57 microphysical and meteorological measurements is shown in Figure 2. The top two panels of this figure show the ER-2 CPL lidar 532 nm attenuated backscatter and extinction retrieval data along the flight segment AB identified in Figure 1, with the WB-57 altitude overplotted (red) at the closest (lat/lon) location to the ER-2. The bottom panels show the in situ data from the WB-57 taken along the same segment approximately an hour after the ER-2. Because the 2D-S probe is directly sensitive to the particle cross-sectional area distribution, the extinction coefficients presented here are twice the integrated area distribution (i.e., $2\pi r/\lambda >> 1$ and $Q_{ext} = 2$). To estimate IWC, a mass-dimensional relationship must be assumed. The mass as a function of area relationship from Baker and Lawson [2006] is used for particles larger than ~ 50 μm, whereas spherical particles are assumed for sizes smaller than 50 μm.

As can be seen from Figure 2, the SVC layer has a large horizontal extent, and is extremely tenuous. The layer is present in the CPL backscatter data from ~12:40 – 13:15 UT, which corresponds to a horizontal distance of over 400 km at the ER-2 speed. As indicated by the CPL and microphysical measurements aboard the WB-57, this SVC layer was extremely tenuous, with number concentration, optical extinction, optical depth, and IWC values less than 10 L^{-1}, 0.01 km^{-1}, 0.004, and 5 x 10^{-3} g m^{-3}, respectively. For comparison, the mean values from CR-AVE reported by *Lawson et al*. [2008] are 66 L^{-1}, 0.009 km^{-1}, and 5.5 x 10^{-5} g m^{-3}. It is worth noting that the TC4 values are below the detection limit for CALIPSO [$\tau \approx 0.01$, *Yang et al.,* JGR, in press], indicating that clouds with properties similar to the one discussed here have been and will be unaccounted for in global satellite-based studies.

As shown in Figure 2, the in-cloud water vapor values are in the range of 6 – 10 ppmv, with relative humidity with respect to ice (RH_i) ~ 80 – 130%, depending on the instrument used. In general, the JLH values are ~100 % RH_i, whereas the HW values are closer to 120%. For each instrument, the in-cloud water vapor values span a range of slightly more than 2 ppmv, and the offset between the two primary water vapor instruments (JLH and HW) is approximately 1 ppmv. Neither instrument observed large RH_i (i.e., > ~ 160%) in these SVC, in contrast with the CR-AVE measurements where supersaturations of ~ 200% were noted inside SVC by the HW and the Harvard ICOS instruments [*Jensen et al.*, 2008; *Lawson et al.*, 2008]. This difference may reflect the fact that the TC4 SVC were warmer than during CR-AVE (196-198 K as opposed to < 190 K for CR-AVE), and there is a well-documented increase in the frequency of observed supersaturation as temperature decreases for temperatures below 200 K [*Gao et al.*, 2004; *Kraemer et al.*, 2009].

Figure 3 shows in situ vertical profiles of the 4 passes through the SVC layer. The temperature profile and IWC/extinction profiles show that the top of the SVC layer lies immediately below the cold-point tropopause (within ~ 0 – 200 m). That SVC reside near the cold-point has been recognized by previous studies, but their proximity to the cold-point has not been illustrated as clearly as in the case presented here. This property is relevant to the dehydration potential of these types of clouds, and suggests that if irreversible dehydration is occurring in these clouds, it is likely the last occurrence before the air ascends into the stratosphere.

The vertical profiles also illustrate several salient features of the SVC. First, they are clearly associated with a region of the atmosphere that is high in relative humidity and of limited vertical extent. In Figure 3, both the JLH and HW instruments indicate that the SVC reside in a region of the atmosphere that is at or above supersaturation, with subsaturated regions below cloud and a limited region of saturation just above cloud. The vertical thickness of the SVC layer ranges from ~300 – 800 m, with an average of 500 m for the four passes. Another interesting feature of these clouds is that there is a decrease with height of effective particle size that is commonly observed in ice clouds. This behavior is similar to that observed in de *Reus et al.* [2008], and is expected when the time scale for gravitational size sorting is longer than the cloud lifetime. Also, both Figures 2 and 3 illustrate that there is considerable horizontal heterogeneity of the SVC layer, with peak extinctions and τ for the various passes spanning almost an order of magnitude.

Finally, CPI imagery from the SVC encounters is shown in Figure 4. These images are almost entirely quasi-spherical, similar to the CR-AVE CPI data, but different from the complex columnar and trigonal shapes observed in the Western Pacific by Heymsfield [1986].

Because very few particle size distribution measurements have been made in SVC, the shapes of the size distributions are not well constrained by in situ measurements. Here, we compare the TC4 SVC case with previous in situ measurements from the Western Pacific in 1973 [FSSP-300 and replicator data, *Heymsfield and McFarquhar*, 1996; *McFarquhar et al.*, 2000], APE-THEOSO in 1999 [FSSP-300, *Thomas et al.*, 2002], CR-AVE in 2006 [2D-S, *Lawson et al.*, 2008], and the African Monsoon Multidisciplinary Analysis (AMMA) campaign in 2006. Average SVC size distributions in terms of number concentration from each of these field studies are plotted in Figure 5 along side an average over the 6 August 2007 TC4 passes. The general shapes of these size distributions look remarkably similar to one another given the wide range of geographical locations, seasons, and instruments from which they were taken. The TC4 size distribution is somewhat of an outlier in this figure, but this is to be expected given the tenuousness of the SVC layer.

3. SVC radiative heating rates

In this section, the LW and SW radiative heating rates are computed for both clear-sky and (SVC) cloudy-sky cases, and the cloud radiative effect due to the SVC layer is also calculated. Results plotted here are from the Rapid Radiative Transfer Model [RRTM, *Mlawer and Clough*, 1997; *Mlawer et al.*, 1997]. Nearly identical results were also found from Libradtran [*Mayer and Kylling*, 2005] and the Fu-Liou radiative transfer models [*Fu and Liou*, 1993]. RRTM uses a correlated-k method for gaseous absorption, the CKD 2.4 water vapor continuum model [*Clough et al.*, 1989], and cloud ice parameterizations based on an effective size and water content [*Fu et al.*, 1998; *Fu*, 1996]. The key model input parameters relevant to this study are the vertical profiles of atmospheric temperature, ozone, water vapor, and cloud microphysical properties including the ice water path and a generalized effective diameter for ice [D_{ge}, e.g., eqs. 3.11-3.12, *Fu*, 1996].

The vertical profiles input into the model are shown in Figure 6. For temperature, we use the vertical profile from a Vaisala RS-92 radiosonde launched at 12 UT on 6 August from the Juan Santamaria Airport in Alajuela, Costa Rica. The vertical temperature profile agrees very well with the MMS temperature measurements aboard the WB-57 (within 2 K from the surface to the peak WB-57 altitude), but is used because it extends up to ~10 mb. Above this level until 1 mb, the Microwave Limb Sounder (MLS) temperature profile from the nearest Aura overpass (within 500 km) at 7 UT is used. Ozone data are provided by an ECC ozonesonde launched from Alajuela on 7 August 2007 at 6 UT. As with the temperature profile, MLS data are used above ~ 10 mb.

Water vapor are provided by the JLH from 300 mb to the peak WB-57 altitude. Below 300 mb, cryogenic frost-point hygrometer [CFH, *Vomel et al.*, 2007] data are used from the same payload as the ozonesonde. MLS water vapor data are used for altitudes above the WB-57. It should be noted that these three instruments agree well in their overlap region on this day.

The cloudy-sky radiative heating rates are calculated for each of the four passes through the SVC layer using the 2D-S microphysical data as input. The cloud microphysical properties input into the model are IWP (i.e., vertically integrated IWC over the cloud layer) and mean effective size. The IWP values range from 8.8×10^{-4} g m^{-2} to 1.2×10^{-2} g m^{-2}, with D_{ge} from 16 μm to 25 μm (r_e from 10 μm to 16 μm). The τ_{vis} calculated using the Fu paramaterization range from about 10^{-4} to 10^{-3} over the four passes, which is consistent with the range of τ_{vis} calculated from both the 2D-S data and retrieved from the CPL lidar backscatter. The mean CPL τ_{vis} (± 1σ) during the entire period shown in Figure 2 is 6.4 x 10^{-3} (± 3.3 x 10^{-3}).

The radiative heating rate results are shown in Figure 6. The clear-sky LW, SW, and total (LW+SW) radiative heating rates are shown for the first and third SVC encounters, as they represent the optically thinnest and thickest cases, respectively. The SVC layer is very close to the level of net zero radiative heating, and clouds produce a positive (warming) local perturbation to the radiative heating rate, mostly due to LW heating. The net perturbations range from 0.005 K day^{-1} to 0.12 K day^{-1}. These heating rate values are significantly smaller than the values presented by *McFarquhar et al.* [2000] and *Comstock et al*. [2002], who calculated perturbations of ~ 0.5 – 2 K day^{-1} for SVC. However, the τ_{vis} for the clouds considered in these previous studies were ~ 0.004 – 0.02, and are significantly larger than those observed on this flight.

Finally, the net TOA cloud radiative effect, defined here as the cloudy minus clear sky difference in total (SW+LW) upward flux, is calculated. The thinnest three passes through the layer (passes 1,2,4) produce radiative effects < 0.001 W m^{-2}, which may not be significant given the numerical accuracy of the model. The radiative effect from the thickest pass (#3) was of 0.015 W m^{-2}, with a 0.154 W m^{-2} LW effect mostly compensated for by a 0.139 W m^{-2} SW effect in the model. These results are much smaller than previous estimates for SVC [*Comstock et al.*, 2002; *McFarquhar et al.*, 2000], which were ~ 1 W m^{-2}. However, our results are merely reflective of the thinness of this particular SVC, and should not be construed as being in disagreement with previous work. The RRTM model gives similar values for cloud radiative effects if one inputs optical depths similar to these previous studies.

4. SVC climatology from TC4

To address whether the extreme thinness of the SVC layer observed during the 6 August 2007 TC4 flight represents a unique type of cloud or merely the tail end of a smooth distribution of SVC optical properties, we analyze statistics from the ER-2 CPL for the entire TC4 mission.

The ER-2 flew 11 flights based out of San Jose, Costa Rica between July 17 and August 8, 2007. During these flights, the CPL obtained 51 hours of data in the tropics (see Figure 1), corresponding to approximately 37,000 km of distance. Many of these flights were coordinated with the DC-8 as it sampled clouds lower in the atmosphere, so in general the ER-2 CPL data in the mid-troposphere are likely biased towards cloudy conditions at DC-8 altitudes (< 12 km). However, it is less likely that CPL SVC data are significantly biased in terms of their sampling of SVC vs. SVC-free air, as the SVC formation mechanisms and persistence are largely decoupled from lower atmospheric cloudiness.

The CPL data used here have been analyzed using a layer detection algorithm that detects up to 10 layers of aerosol and/or cloud [*Hlavka et al.*, submitted]. The statistics presented here are from the uppermost cloud layer detected by the CPL. During the TC4 mission, SVC with $\tau_{532} < 0.03$ and cloud bases above 15 km were present 4% of the time. This value is lower than the most directly comparable estimate of 29% provided by *McFarquhar et al*. [2000]. The *McFarquhar et al.* estimate is based on airborne lidar data taken during the Central Equatorial Pacific Experiment (CEPEX) in February, 1993 near Fiji, and the data were screened for clouds with bases above 15 km. Some difference between the TC4 and CEPEX SVC frequencies is expected given the seasonal/geographic differences and the regional variations in SVC frequency indicated by satellite measurements [*Winker and Trepte*, 1998]. Because an optical extinction retrieval was not used with the CEPEX data, clouds were not explicitly filtered out on the basis of optical depth as in the TC4 CPL data. However, removing the $\tau_{532} < 0.03$ requirement from our estimate only raises the cloud occurrence frequency to 5%. We suspect that the discrepancy is due to the colder near-tropopause temperatures during CEPEX related to both geographic and seasonal differences between equatorial Western winter and Eastern Pacific summer. Several other studies have obtained estimates of ~50% occurrence frequency for optically thin tropical cirrus [*Nee et al.*, 1998; *Prabhakara et al.*, 1988; *Wang et al.*, 1994], but these values are not directly comparable because the studies did not specifically consider SVC near the tropopause. These estimates are actually quite similar to the upper tropospheric cloud occurrence frequency from the CPL during TC4, which was 42% [*Hlavka et al.*, submitted].

In addition to the frequency statistics, Figure 7 shows histograms of various cloud parameters retrieved from CPL data during TC4. Figures 7a-c show 2D histograms of SVC ($\tau < 0.03$) properties such as τ and thickness. The median, mean, and standard deviation of optical depth for SVC (all clouds) with base heights above 15 km is 0.0016 (0.0023), 0.0035 (0.17), and 0.0050 (0.57). Excluding clouds with $\tau > 0.1$, which was effectively the value chosen by *McFarquhar et al.* [2000] in their analysis of tropopause cirrus, the TC4 mean (median) value is 0.0069 (0.0018), compared to their mean value of 0.0045. As evidenced by these numbers and the distributions in Figure 7, which are plotted on a log abcissa, the distributions of tropopause cirrus are highly skewed, so caution should be taken when interpreting the radiative implications of these results.

Figure 7 also contains statistics concerning how τ and cloud thickness vary with height. In general, both τ and cloud thickness decrease with height. However, because a decrease in thickness would lead to a decrease in τ for a given β, it is possible that merely a thinning of the cloud layers with increasing height could explain the trend in τ. But as shown in Figure 7c, the cloud-layer mean β (defined as $\tau/\Delta z$) also decreases with height. Thus, the decrease with height of τ is due to both decreases in cloud thickness as well as decreases in extinction. This is not a surprising result due to the lack of available water for condensation at these temperatures, and has been qualitatively seen in other studies [e.g., in cirrus IWC, *Schiller et al.*, 2008].

5. Conclusions

Subvisible cirrus clouds were observed frequently near the tropopause by the cloud physics lidar aboard the NASA ER-2 aircraft during the TC4 field campaign. On the 6 August flight, the CPL indicated an extensive subvisible cirrus deck, and the WB-57 aircraft was directed to porpoise through the layer, making in situ measurements along the same track flown by the ER-2 approximately an hour earlier. From these maneuvers, vertical profiles of temperature, water vapor, and microphysical properties including extinction, IWC, and effective size were made from aboard the WB-57. These measurements add to the relatively sparse set of in situ SVC measurements that exist, and are shown to be qualitatively similar to previous studies. However, there are several points regarding tropopause SVC that have been illustrated by the TC4 data in a manner more clearly than in previous studies.

The TC4 SVC measurements support the idea that a distinct class of subvisible cirrus clouds exists within a relatively narrow vertical layer just below the tropical cold-point tropopause. The data clearly show that these clouds are on the order of ~500 m thick, with cloud tops < 200 m below the local cold-point tropopause, and with $RH_i \geq 100$ %. Given their proximity to the cold point and location within a region of net radiative heating, these clouds have the potential to play a role in dehydration of air as it enters the stratosphere. However, because these measurements represent a snapshot in time, it is not possible to know whether or not irreversible dehydration occurred in this specific cloud layer. If irreversible dehydration is occurring in this air parcel as it ascends through the cold-point, then an upper-bound estimate is given by the IWC of the SVC cloud, which is at most 0.5 ppmv for the 6 August case.

It is also possible that these clouds contribute to a hydration of the stratosphere through their positive radiatiave heating perturbations via the mechanism proposed by *Rosenfield et al*. [1998]. It is worth noting that the upper limit of the radiative heating rates presented here (~ 0.1 K day^{-1}) is similar to values from *Rosenfield et al*. (0.1 – 0.2 K day^{-1}) that caused a 1 ppmv increase in stratospheric water in their model. Thus, although the thinnest of SVC clouds may have a negligible instantaneous radiative forcing value, their localized LW radiative heating rate perturbations may still have the potential to affect stratospheric humidity.

Finally, the TC4 in situ and CPL SVC data highlight the fact that estimates of the occurrence frequency of thin tropopause cirrus from satellite-borne instruments such as CALIPSO are likely to miss a significant fraction of subvisible cirrus clouds. As an example, < 10% of ice clouds detected by CALIPSO have $\tau < 0.01$ [*Yang and Fu*, in press], whereas in the TC4 CPL data set the number is 37%. A detailed intercomparison between cirrus statistics from CALIPSO and more sensitive airborne lidars such as the CPL would be a fruitful exercise to better quantify these differences.

Acknowledgements

The authors would like to thank the efforts of the TC4 mission planners and instrument investigators, as well as the pilots and staff of the DC-8, WB-57, and ER-2 aircraft. The authors would also like to acknowledge the CPL instrument team, led by P.I. Matt McGill. SMD would like to thank Qiong Yang for assistance with the Fu-Liou radiation model, and Anthony Bucholtz for discussions on SVC heating rates. SMD acknowledges support from NASA grant.

References:

Lawson, R. P., B. A. Baker, C. G. Schmitt, and T. L. Jensen (2001), An overview of microphysical properties of Arctic clouds observed in May and July 1998 during FIRE ACE, *Journal of Geophysical Research-Atmospheres*, *106*, 14989-15014.

Baker, B., and R. P. Lawson (2006), Improvement in determination of ice water content from two-dimensional particle imagery. Part I: Image-to-mass relationships, *Journal of Applied Meteorology and Climatology*, *45*(9), 1282-1290.

Clough, S. A., et al. (1989), Line shape and the water vapor continuum, *Atmospheric Research*, *23*(3-4), 229-241.

Comstock, J. M., et al. (2002), Ground-based lidar and radar remote sensing of tropical cirrus clouds at Nauru Island: Cloud statistics and radiative impacts, *Journal of Geophysical Research-Atmospheres*, *107*(D23), -.

Corti, T., et al. (2006), The impact of cirrus clouds on tropical troposphere-to-stratosphere transport, *Atmospheric Chemistry and Physics*, *6*, 2539-2547.

de Reus, M., et al. (2008), Evidence for ice particles in the tropical stratosphere from in-situ measurements, *Atmos. Chem. Phys. Discuss.*, *8*(6), 19313-19355.

Dvortsov, V. L., and S. Solomon (2001), Response of the stratospheric temperatures and ozone to past and future increases in stratospheric humidity, *Journal of Geophysical Research-Atmospheres*, *106*(D7), 7505-7514.

Forster, P. M. D., and K. P. Shine (2002), Assessing the climate impact of trends in stratospheric water vapor, *Geophysical Research Letters*, *29*(6), -.

Fu, Q., and K. N. Liou (1993), Parameterization of the Radiative Properties of Cirrus Clouds, *Journal of the Atmospheric Sciences*, *50*(13), 2008-2025.

Fu, Q., et al. (1998), An accurate parameterization of the infrared radiative properties of cirrus clouds for climate models, *Journal of Climate*, *11*(9), 2223-2237.

Fu, Q. A. (1996), An accurate parameterization of the solar radiative properties of cirrus clouds for climate models, *Journal of Climate*, *9*(9), 2058-2082.

Gao, R. S., et al. (2004), Evidence that nitric acid increases relative humidity in low-temperature cirrus clouds, *Science*, *303*(5657), 516-520.

Haladay, T., and G. Stephens (2009), Characteristics of tropical thin cirrus clouds deduced from joint CloudSat and CALIPSO observations, *Journal of Geophysical Research-Atmospheres*, *114*, -.

Heymsfield, A. J. (1986), Ice Particles Observed in a Cirriform Cloud at -83-Degrees-C and Implications for Polar Stratospheric Clouds, *Journal of the Atmospheric Sciences*, *43*(8), 851-855.

Heymsfield, A. J., and G. M. McFarquhar (1996), High albedos of cirrus in the tropical Pacific warm pool: Microphysical interpretations from CEPEX and from Kwajalein, Marshall islands, *Journal of the Atmospheric Sciences*, *53*(17), 2424-2451.

Hlavka, D. L., et al. (submitted), Vertical cloud climatology during TC4 derived from high-altitude aircraft merged lidar and radar profiles, *Journal of Geophysical Research-Atmospheres*.

Jensen, E. J., et al. (1996), Dehydration of the upper troposphere and lower stratosphere by subvisible cirrus clouds near the tropical tropopause, *Geophysical Research Letters*, *23*(8), 825-828.

Jensen, E. J., et al. (2008), Formation of large (similar or equal to 100 mu m) ice crystals near the tropical tropopause, *Atmospheric Chemistry and Physics*, *8*(6), 1621-1633.

Kraemer, M., et al. (2009), Ice supersaturations and cirrus cloud crystal numbers, *Atmos. Chem. Phys.*, *9*(11), 3505-3522.

Lawson, R. P., et al. (2001), An overview of microphysical properties of Arctic clouds observed in May and July 1998 during FIRE ACE, *Journal of Geophysical Research-Atmospheres*, *106*(D14), 14989-15014.

Lawson, R. P., et al. (2006), The 2D-S (Stereo) probe: Design and preliminary tests of a new airborne, high-speed, high-resolution particle Imaging probe, *Journal of Atmospheric and Oceanic Technology*, *23*(11), 1462-1477.

Lawson, R. P., et al. (2008), Aircraft measurements of microphysical properties of subvisible cirrus in the tropical tropopause layer, *Atmospheric Chemistry and Physics*, *8*(6), 1609-1620.

Luo, B. P., et al. (2003), Dehydration potential of ultrathin clouds at the tropical tropopause, *Geophysical Research Letters*, *30*(11), -.

May, R. D. (1998), Open-path, near-infrared tunable diode laser spectrometer for atmospheric measurements of H2O, *Journal of Geophysical Research-Atmospheres*, *103*(D15), 19161-19172.

Mayer, B., and A. Kylling (2005), Technical note: The libRadtran software package for radiative transfer calculations - description and examples of use, *Atmospheric Chemistry and Physics*, *5*, 1855-1877.

McFarquhar, G. M., et al. (2000), Thin and subvisual tropopause tropical cirrus: Observations and radiative impacts, *Journal of the Atmospheric Sciences*, *57*(12), 1841-1853.

McGill, M., et al. (2002), Cloud Physics Lidar: instrument description and initial measurement results, *Applied Optics*, *41*(18), 3725-3734.

Mlawer, E. J., and S. A. Clough (1997), On the extension of rapid radiative transfer model to the shortwave region, paper presented at 6th Atmospheric Radiation Measurement (ARM) Science Team Meeting, U.S. Department of Energy, CONF-9603149.

Mlawer, E. J., et al. (1997), Radiative transfer for inhomogeneous atmospheres: RRTM, a validated correlated-k model for the longwave, *Journal of Geophysical Research-Atmospheres*, *102*(D14), 16663-16682.

Nee, J. B., et al. (1998), Lidar observation of the cirrus cloud in the tropopause at Chung-Li (25 degrees N, 121 degrees E), *Journal of the Atmospheric Sciences*, *55*(12), 2249-2257.

Prabhakara, C., et al. (1988), Thin Cirrus Clouds - Seasonal Distribution over Oceans Deduced from Nimbus-4 Iris, *Journal of Applied Meteorology*, *27*(4), 379-399.

Rosenfield, J. E., et al. (1998), The impact of subvisible cirrus clouds near the tropical tropopause on stratospheric water vapor, *Geophysical Research Letters*, *25*(11), 1883-1886.

Schiller, C., et al. (2008), Ice water content of Arctic, midlatitude, and tropical cirrus, *Journal of Geophysical Research-Atmospheres*, *113*, -.

Scott, S. G., et al. (1990), The Meteorological Measurement System on the Nasa Er-2 Aircraft, *Journal of Atmospheric and Oceanic Technology*, *7*(4), 525-540.

Stephens, G. L., et al. (1990), The Relevance of the Microphysical and Radiative Properties of Cirrus Clouds to Climate and Climatic Feedback, *Journal of the Atmospheric Sciences*, *47*(14), 1742-1753.

Thomas, A., et al. (2002), In situ measurements of background aerosol and subvisible cirrus in the tropical tropopause region, *Journal of Geophysical Research-Atmospheres*, *107*(D24), -.

Toon, O. B., et al. (this issue), Planning and Implementation of the Tropical Composition, Cloud and Climate Coupling Experiment (TC4), *Journal of Geophysical Research-Atmospheres*.

Vomel, H., et al. (2007), Accuracy of tropospheric and stratospheric water vapor measurements by the cryogenic frost point hygrometer: Instrumental details and observations, *Journal of Geophysical Research-Atmospheres*, *112*(D8), -.

Wang, P.-H., et al. (1994), Tropical high cloud characteristics derived from SAGE II extinction measurements, *Atmospheric Research*, *34*(1-4), 53-83.

Weinstock, E. M., et al. (1994), New Fast-Response Photofragment Fluorescence Hygrometer for Use on the Nasa Er-2 and the Perseus Remotely Piloted Aircraft, *Review of Scientific Instruments*, *65*(11), 3544-3554.

Winker, D. M., and C. R. Trepte (1998), Laminar cirrus observed near the tropical tropopause by LITE, *Geophysical Research Letters*, *25*(17), 3351-3354.

Yang, Q., and Q. Fu (in press), Radiative Impacts of Clouds in the Tropical Tropopause Layer, *Journal of Geophysical Research-Atmospheres*.

Figure 1. (Top) The WB-57 and ER-2 flight tracks on 6 August 2007. Both planes flew along segment AB during their outbound legs, with the WB-57 lagging about 45 minutes behind the ER-2. (Bottom) ER-2 flight tracks for all 11 TC-4 flights based out of San Jose, Costa Rica.

Figure 2. Timeseries plots of subvisible cirrus measurements taken during the 6 August 2007 TC4 ER-2 and WB-57 flights, plotted along the segment A-B shown in Figure 1. Data are the (a & b) ER-2 CPL attenuated backscatter and extinction at 532 nm, (c) in situ temperature and altitude from the WB-57 MMS (altitude color-coded by 2D-S IWC), (d & e) water vapor and RH_i from the JLH and Harvard instruments on the WB-57, (f & g) visible optical extinction and ice water content from the 2D-S on the WB-57.

Figure 3. Vertical profiles taken from the four passes made through the subvisible cirrus layer on 6 August 2007 by the WB-57, and CPL data from the ER-2. Thick solid lines are in-cloud data, and dotted lines are clear-air data. All profiles are color-coded by the pass number through the SVC layer, except for the CPL data from the ER-2, which are presented as a 2D probability distribution function.

Figure 4. CPI imagery taken during the four SVC passes made by the WB-57 on 6 Aug 2007.

Figure 5. Plot of mean size distributions from tropical near-tropopause subvisible cirrus from various field campaigns.

Figure 6. (top) Profiles of temperature, water vapor, ozone, and IWC used for radiative heating rate calculations for the 6 August 2007 TC4 subvisible cirrus case. (bottom) Calculated LW and SW clear-sky heating rates, and the minimum and maximum SVC heating rate perturbations corresponding to the optically thinnest and thickest passes through SVC during the 6 August flight.

Figure 7. (a-c) 2D histograms of SVC ($\tau < 0.03$) observed by the CPL during TC4. (d) Histograms of τ for clouds with base-heights above 15 km and $\tau < 0.1$ from CEPEX and TC4. The means and standard deviations for these distributions are given on the plot.

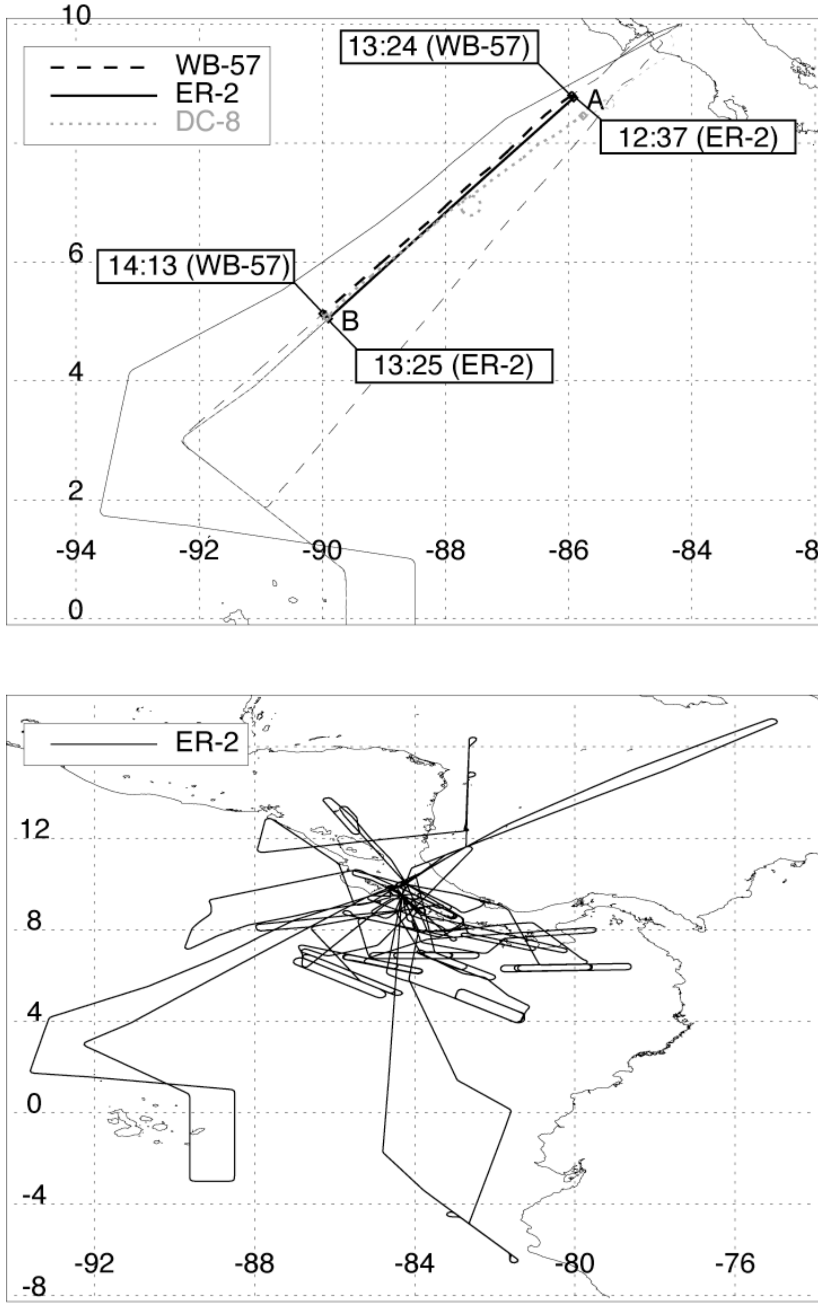

Figure 1. (Top) The WB-57 and ER-2 flight tracks on 6 August 2007. Both planes flew along segment AB during their outbound legs, with the WB-57 lagging about 45 minutes behind the ER-2. (Bottom) ER-2 flight tracks for all 11 TC-4 flights based out of San Jose, Costa Rica.

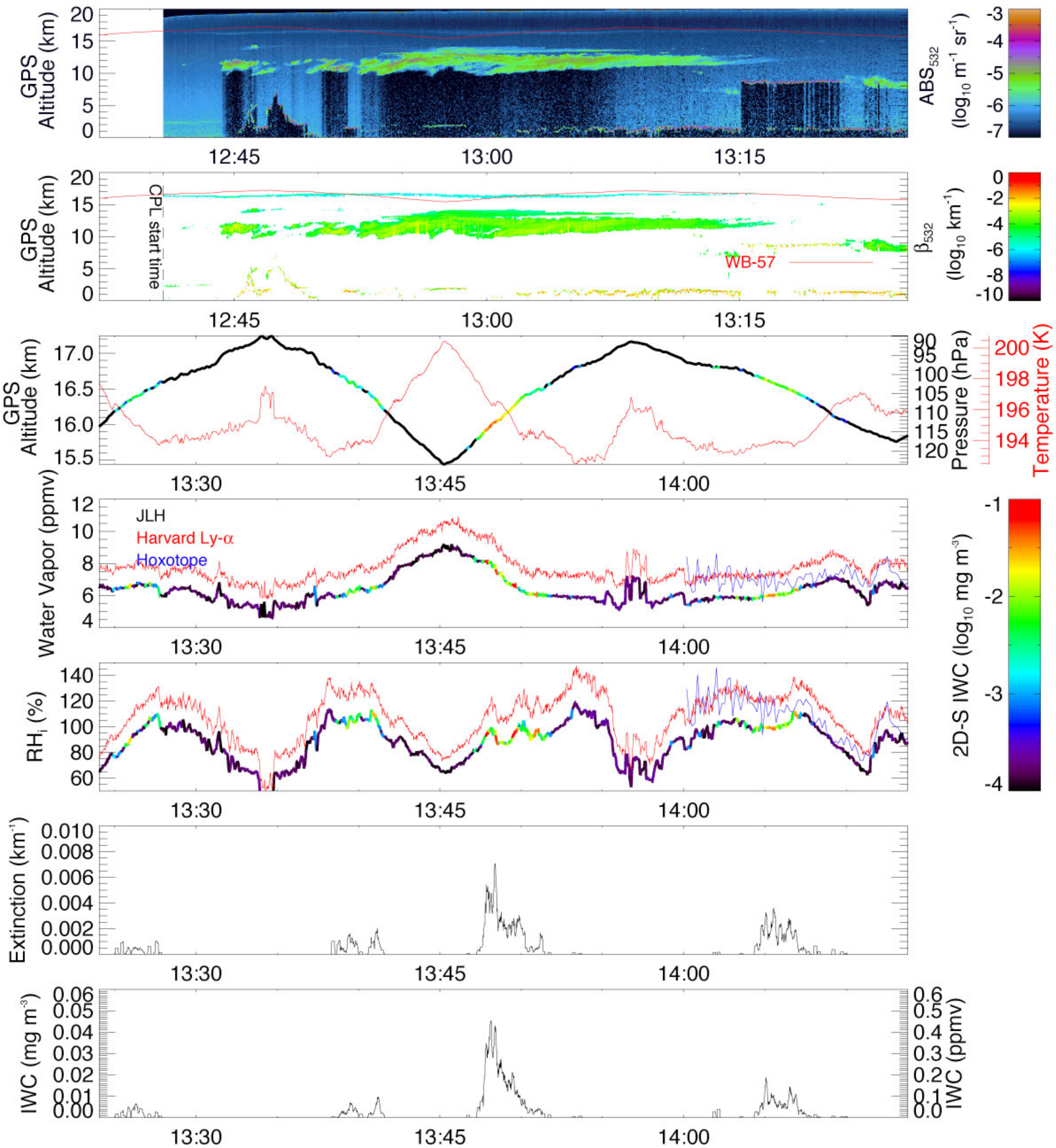

Figure 2. Timeseries plots of subvisible cirrus measurements taken during the 6 August 2007 TC4 ER-2 and WB-57 flights, plotted along the segment A-B shown in Figure 1. Data are the (a & b) ER-2 CPL attenuated backscatter and extinction at 532 nm, (c) in situ temperature and altitude from the WB-57 MMS (altitude color-coded by 2D-S IWC), (d & e) water vapor and

RH_i from the JLH and Harvard instruments on the WB-57, (f & g) visible optical extinction and ice water content from the 2D-S on the WB-57.

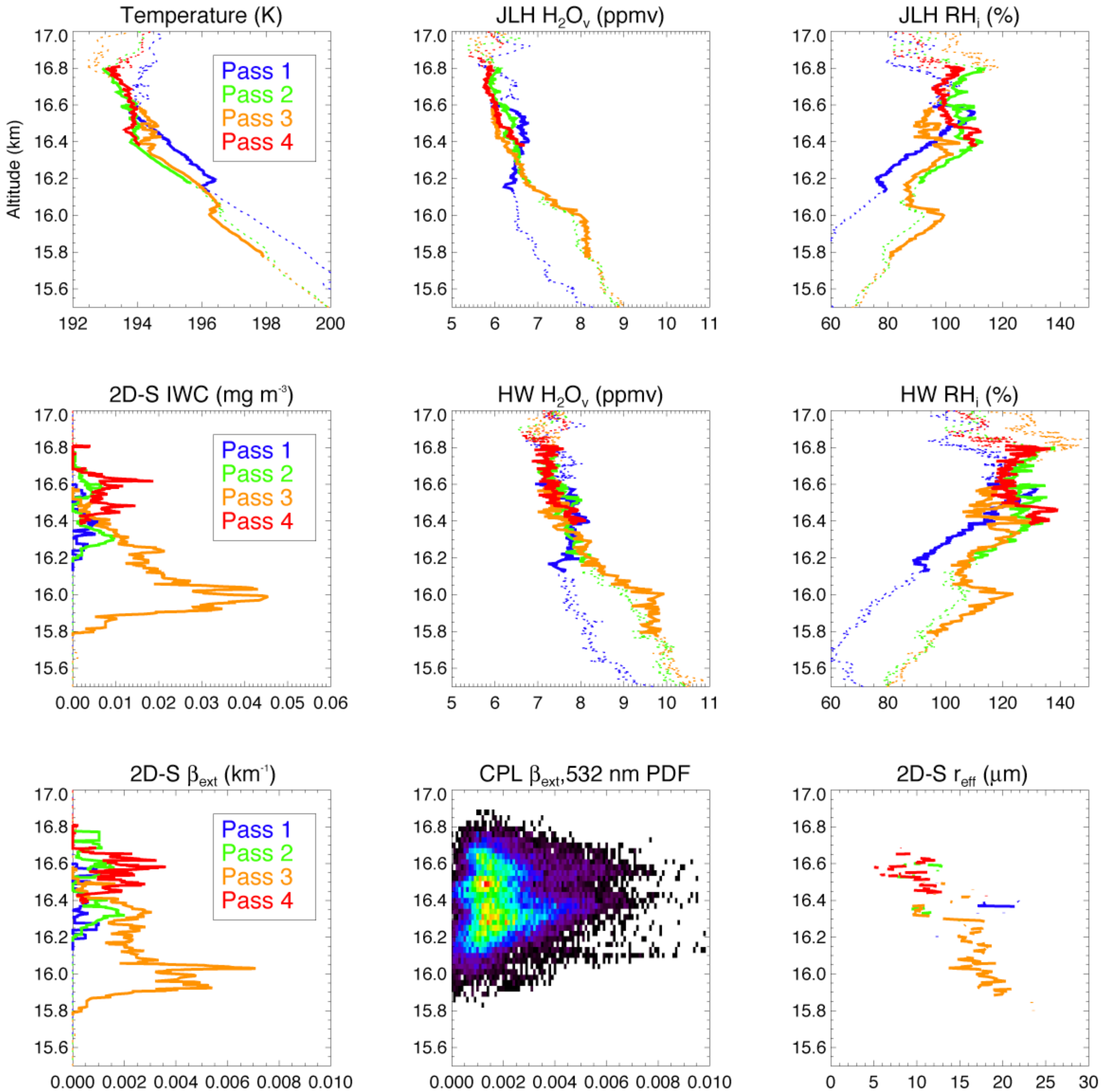

Figure 3. Vertical profiles taken from the four passes made through the subvisible cirrus layer on 6 August 2007 by the WB-57, and CPL data from the ER-2. Thick solid lines are in-cloud data, and dotted lines are clear-air data. All profiles are color-coded by the pass number through the SVC layer, except for the CPL data from the ER-2, which are presented as a 2D probability distribution function.

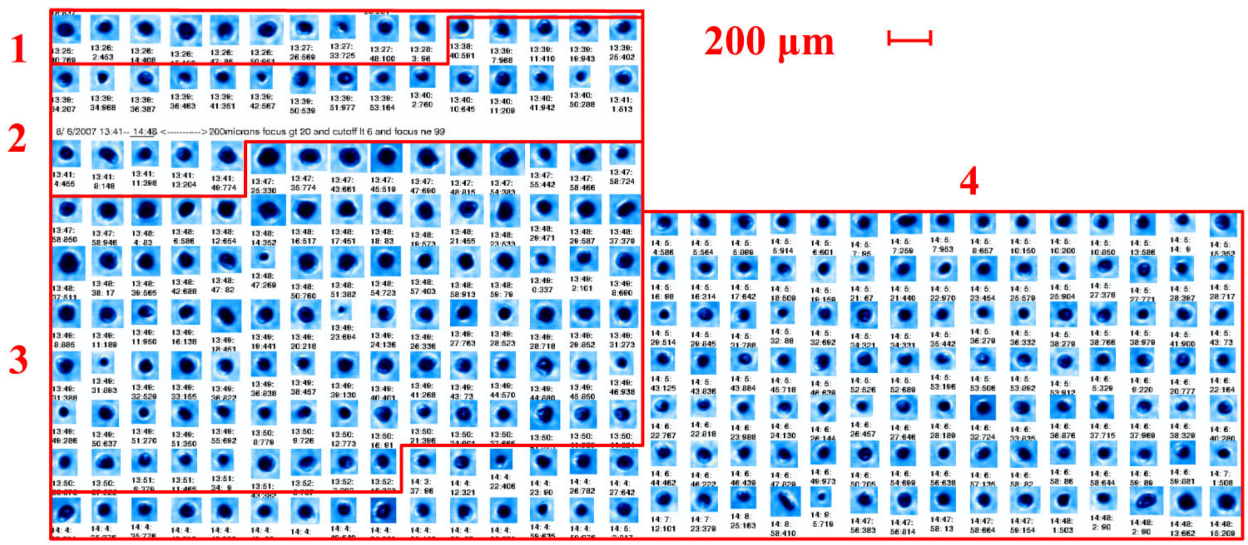

Figure 4. CPI imagery taken during the four SVC passes made by the WB-57 on 6 Aug 2007.

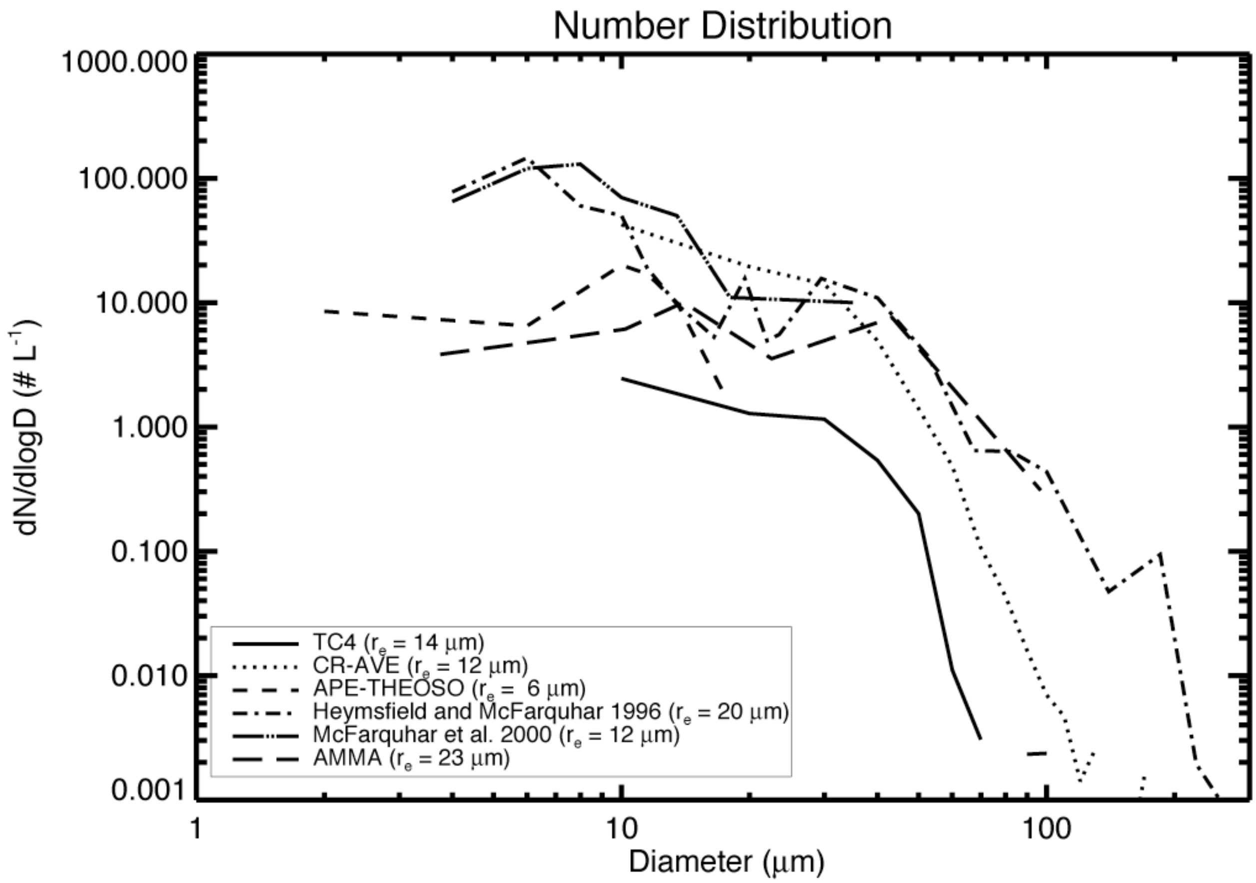

Figure 5. Plot of mean size distributions from tropical near-tropopause subvisible cirrus from various field campaigns.

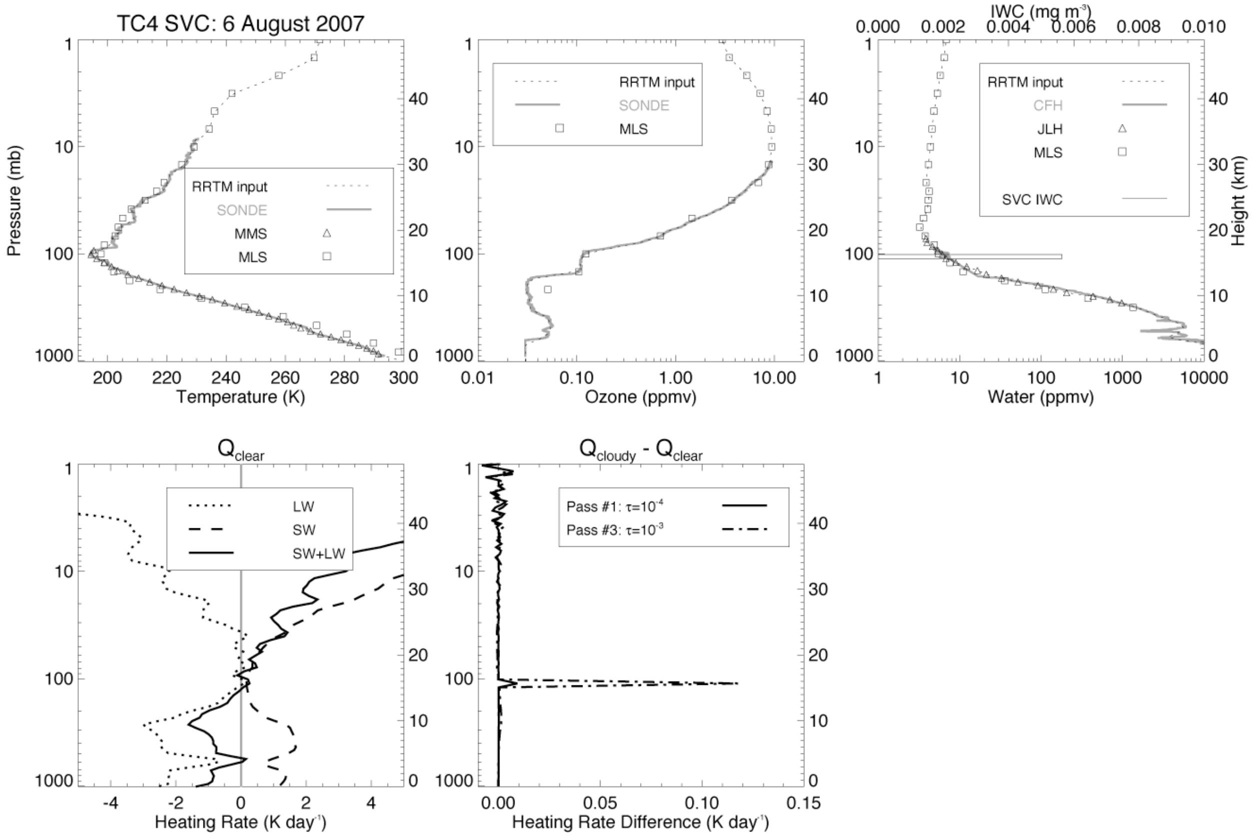

Figure 6. (top) Profiles of temperature, water vapor, ozone, and IWC used for radiative heating rate calculations for the 6 August 2007 TC4 subvisible cirrus case. (bottom) Calculated LW and SW clear-sky heating rates, and the minimum and maximum SVC heating rate perturbations corresponding to the optically thinnest and thickest passes through SVC during the 6 August flight.

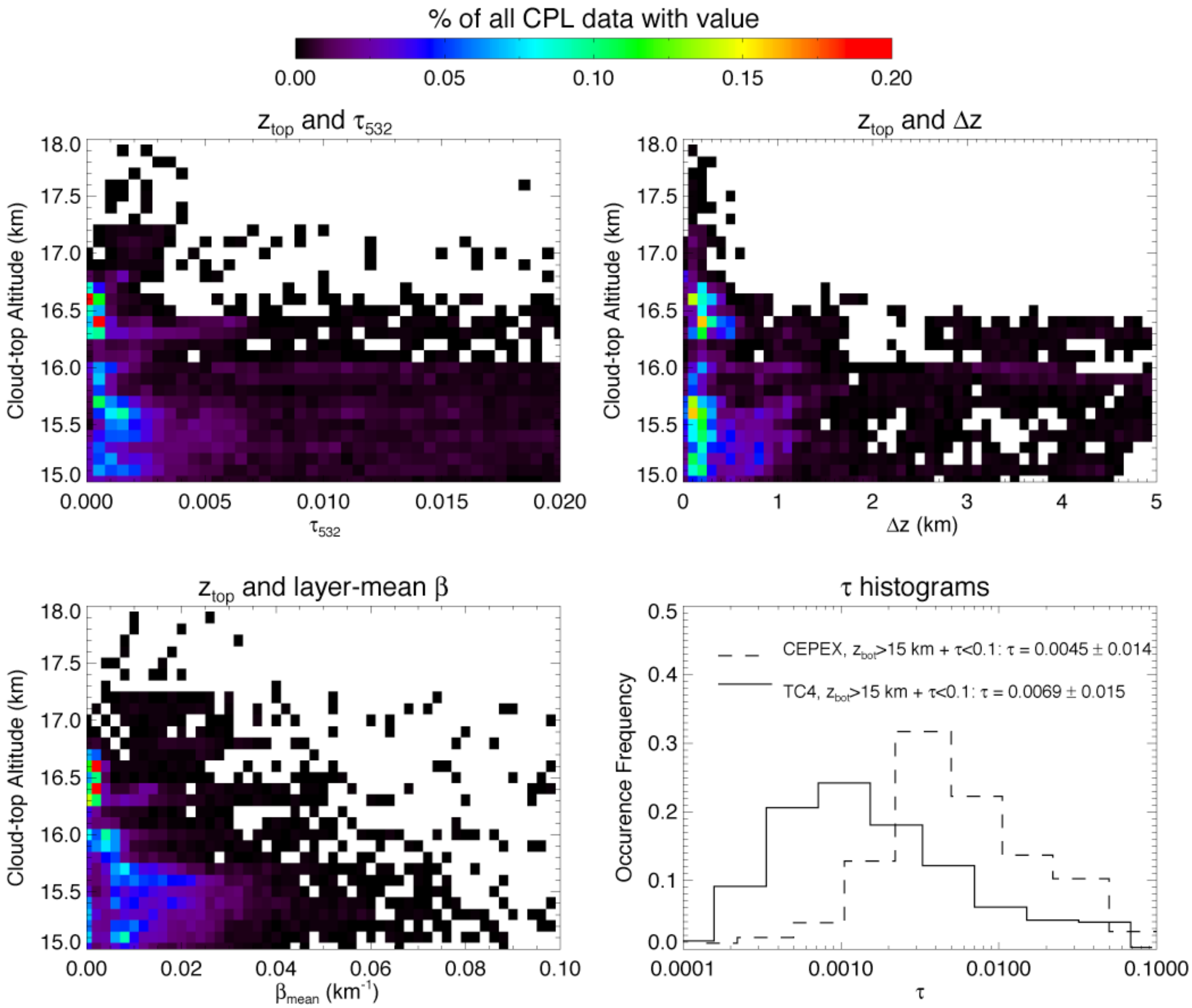

Figure 7. (a-c) 2D histograms of SVC ($\tau < 0.03$) observed by the CPL during TC4. (d) Histograms of τ for clouds with base-heights above 15 km and $\tau < 0.1$ from CEPEX and TC4. The means and standard deviations for these distributions are given on the plot.